Article

Not peer-reviewed version

Experimental Testing Results on Critical Components for Mol-ten Salt-Based CSP Systems

Valeria Russo *, Giuseppe Petroni, Francesco Rovense *, Mauro Giorgetti, Giuseppe Napoli, Gianremo Giorgi, Walter Gaggioli

Posted Date: 2 January 2025

doi: 10.20944/preprints202501.0091.v1

Keywords: Binary molten salt mixtures; pressure sensor; bellows seal globe valves

 doi:10.20944/preprints202501.0091.v1

Article

Experimental Testing Results on Critical Components for Molten Salt-Based CSP Systems

Valeria Russo *, Giuseppe Petroni, Francesco Rovense *, Mauro Giorgetti, Giuseppe Napoli, Gianremo Giorgi and Walter Gaggioli

ENEA – Italian National Agency for New Technologies, Energy and Sustainable Economic Development, Via Anguillarese, 301, Rome, 00123, Italy

* Correspondence: valeria.russo@enea.it (V.R.); francesco.rovense@enea.it (F.R.)

Abstract: Concentrated Solar Power (CSP) plants integrated with Thermal Energy Storage (TES) represent a promising renewable energy source for generating heat and power. Binary molten salt mixtures, commonly referred to as Solar Salts, are utilized as effective heat transfer fluids and storage media due to their thermal stability and favorable thermophysical properties. However, these mixtures pose significant challenges due to their high solidification temperatures, around 240 °C, which can compromise the longevity and reliability of critical system components such as pressure sensors and bellows seal globe valves. Thus, it is essential to characterize their performance, assess their reliability under various conditions, and understand their failure mechanisms, particularly in relation to temperature fluctuations affecting the fluid's viscosity. This article discusses experimental tests conducted on a pressure sensor and a bellows seal globe valve, both designed for direct contact with molten salts in CSP environments, at the ENEA Casaccia Research Center laboratory in Rome. The methodology for conducting these experimental tests is detailed, and guidelines are outlined to optimize plant operation. The findings provide essential insights for improving component design and maintenance to minimize unplanned plant downtime. They also offer methodologies for installing measurement instruments and electrical heating systems on the components.

Keywords: binary molten salt mixtures; pressure sensor; bellows seal globe valves.

1. Introduction

The ongoing rise in global average temperatures presents a critical challenge, with 2023 marking the warmest year on record since 1850, with a mean near-surface temperature approximately 1.40 ± 0.12 °C above the historical average [1]. The European Union's major GHG emitters in 2023 included the manufacturing sector (23.5%), households (17.9%), electricity and gas supply (15.5%), agriculture (14.3%), and transportation (12.8%) [2]. To combat these emissions, the EU's REPowerEU plan, initiated in May 2022, aims to boost Renewable Energy Sources (RES) deployment, improving energy conservation and diversifying energy supplies. Legislative enhancements in March 2023 set a new binding RES target of at least 42.5% by 2030, aiming for 45%, nearly doubling the current RES share in the EU [3]. Integrating novel Renewable Energy Sources (RES) into the electric grid is crucial to meet ambitious sustainability goals, but it faces significant challenges due to the intermittent and variable nature of sources like solar photovoltaics and wind energy. This variability introduces unpredictability in power supply, requiring advanced grid management and substantial energy storage solutions to handle fluctuations in production [4]. The non-dispatchable nature of many RES complicates grid integration, presenting load-following and peak-demand management challenges [5]. Financial and policy issues further complicate the financing and regulation of necessary grid enhancements. Concentrated Solar Power (CSP) systems are particularly beneficial due to their Thermal Energy Storage (TES) capability, which allows for electricity generation even during low solar irradiation periods, thus mitigating issues of intermittency and variability. This capability also

 doi:10.20944/preprints202501.0091.v1

enables CSP plants to provide electricity during peak demand times, supporting the integration of other RES types and allowing for efficient hybrid systems deployment [6–10]. TES systems are designed to minimize heat loss by using well-insulated tanks [11] . These tanks hold a Heat Storage Medium (HSM) that retains heat at high temperatures for extended periods, primarily through concentrated solar radiation. The design and operation of TES systems vary, influenced by the type of storage mechanism—sensible heat, latent heat, or chemical state—and the system's specific configurations, including the choice of HSM and the Heat Transfer Fluid (HTF) [12]. In high-temperature energy applications, molten salts are essential due to their excellent heat transfer and storage properties, with various types categorized by their chemical composition, melting points, corrosivity, and application suitability. The most commonly used binary MS mixture in CSP plants is Solar Salt, a non-eutectic mixture of 60% sodium nitrate and 40% potassium nitrate by weight [13–16]. Research on this mixture has been extensive since the 1980s [17]. Solar Salt is primarily favored for its relatively low cost, chemical safety—it is neither toxic nor flammable—and its compatibility with standard stainless steels, which exhibit minimal corrosion [18]. However, its application is limited to a specific temperature range: it begins to crystallize at around 240°C and can be used up to about 565°C before decomposition and other degradation reactions occur [19]. A main challenge is its tendency to solidify when operational temperatures fall below the HTF melting point, which can block flow pathways and severely compromise the functionality and safety of the system [20]. This mixture provides a favorable balance between a low melting point and moderate corrosivity, which can be managed through careful selection of containment materials. Solar Salt is extensively used in CSP plants due to its thermal stability and cost-effectiveness. It is utilized in both the solar collector and the TES system, obviating the need for costly heat exchangers [12]. This configuration allows the solar field to operate at higher temperatures than those achievable with other HTFs, such as thermal oils, thereby reducing the overall cost of the TES system. However, a significant challenge associated with this binary molten salt mixture is its high solidification temperature, which ranges from 220°C to 240°C [21]. This presents issues for the durability and reliability of crucial system components like sensors and valves, essential for the operational integrity and safety of the plant [22].

Further enhancing the diversity of molten salts are ternary nitrate mixtures, which include a third component to adjust the melting point and thermal properties. These salts often melt below 220 °C, expanding their usability in lower temperature applications while maintaining a corrosion profile similar to that of binary salts [23]. These salts typically include combinations of nitrates, chlorides, or fluorides, with common compositions involving sodium nitrate ($NaNO_3$), potassium nitrate (KNO_3), and an additional salt like calcium nitrate ($Ca(NO_3)_2$) or lithium nitrate ($LiNO_3$)[24]. A notable example of a ternary nitrate salt includes the mixture of $NaNO_3$, KNO_3, and $Ca(NO_3)_2$, which has been shown to have a melting point significantly lower than traditional binary salts like Solar Salt. This lower melting point can enhance the operational efficiency of CSP systems by reducing the risk of solidification in the heat transfer system. The melting point of a mixture of ternary nitrates may initially reach about 124 °C and increase slightly after prolonged thermal exposure [25]. Furthermore, the inclusion of components like $LiNO_3$ and $Ca(NO_3)_2$ in ternary mixtures not only reduces the melting point but also affects other thermal properties such as specific heat and thermal stability. These adjustments make ternary salts suitable for TES by potentially widening the operational temperature range and improving heat capacity [24]. Corrosivity is another critical aspect of molten salts that must be managed to ensure the longevity and reliability of CSP systems. Ternary salts can exhibit different levels of corrosiveness depending on their composition and operational conditions. For instance, the addition of lithium and calcium components has been noted to influence the corrosive behavior of these salts, particularly in interaction with construction materials such as stainless steels. The presence of these components can affect the protective oxide layers on metal surfaces, which are crucial for mitigating corrosion at high temperatures [25]. These properties collectively highlight the potential of ternary molten salts to enhance the efficiency and effectiveness of CSP technologies by offering lower operational temperatures, improved heat transfer

 doi:10.20944/preprints202501.0091.v1

characteristics, and potentially less aggressive interactions with container materials. This makes them a promising area for ongoing research and application in renewable energy technologies [26].

Molten chloride salts, such as the mixture of potassium chloride (KCl) and magnesium chloride ($MgCl_2$), are known for their high operational temperatures, typically melting between 400-500 °C. These salts are highly effective in industrial heat treatment processes and metallurgical applications due to their superior heat transfer characteristics at high temperatures. However, they are also notably more corrosive, which necessitates the use of advanced alloy materials or protective coatings to mitigate corrosion risks. This corrosion behavior, particularly in environments like CSP systems where high temperatures are common, has been extensively studied. For example, some research has shown that the corrosion resistance of stainless steel in molten KCl-$MgCl_2$ can be enhanced through the control of impurities and temperature management, but the corrosive nature of these salts at elevated temperatures remains a challenge[27,28]. On the other hand, fluoride-based salts like the FLiNaK mixture, which consists of lithium fluoride, sodium fluoride, and potassium fluoride, exhibit a melting point around 454 °C. These salts are less corrosive compared to chlorides and nitrates, making them more suitable for nuclear applications where they are used as coolants and heat transfer agents within molten salt reactors. Their lower corrosivity and favorable thermal properties contribute to their preference in settings that require long-term stability and minimal material degradation over time [29].

Carbonate salts, particularly eutectic mixtures involving lithium carbonate (Li_2CO_3), potassium carbonate (K_2CO_3), and sodium carbonate (Na_2CO_3), have gained attention in the field of CSP technologies due to their favorable thermophysical properties. These salts typically have a melting point around 397°C and offer a promising balance between high heat capacity and thermal stability, which makes them suitable for TES applications within CSP systems. The relatively lower corrosivity of these salts compared to other molten salts enhances their appeal, as it can lead to reduced maintenance costs and longer lifespans for CSP infrastructure [30,31]. The specific eutectic mixture of Li_2CO_3-K_2CO_3-Na_2CO_3, known for its effective heat transfer and storage capabilities, is not only notable for its operational efficiency but also for its chemical stability under typical CSP operating conditions. However, despite their advantages, the corrosive potential of carbonate salts at high temperatures cannot be completely overlooked. Studies have shown that while these salts are less corrosive than many chloride salts, they still pose challenges, particularly at temperatures exceeding 500°C where they can accelerate corrosion processes in common structural materials used in CSP systems [32,33].

Next-generation CSP TES systems are shifting towards the use of phase change materials (PCMs) capable of operating at temperatures above the traditional maximum of 560°C [34]. Sustaining these higher temperatures necessitates robust corrosion management within PCM-based TES systems. Corrosion significantly compromises thermal performance by causing corrosion products to dissolve into the salt storage media, altering its essential properties. Additionally, scale buildup on heat exchanger surfaces can severely reduce their heat transfer efficiency. Therefore, careful selection of molten salts and rigorous assessment of material compatibility are critical for optimizing these advanced TES systems [35]. The challenges associated with the viscosity of molten salts in CSP plants can lead to significant operational issues, including component failures or malfunctions. These issues often result in unplanned operational downtimes and substantial repair costs. Molten salts, particularly those used for TES in CSP systems, possess properties that not only affect the thermophysical characteristics of the system but also influence the corrosion dynamics of the interacting materials. This interplay between viscosity, heat transfer efficiency, and corrosion can greatly impact the overall durability and efficiency of CSP plant components. Research highlights that the viscosity of molten salts in CSP systems plays a critical role in affecting flow characteristics and heat transfer efficiency. Lower viscosity salts enhance pumpability and reduce the energy needed for circulation, essential for efficient heat transfer. However, the corrosiveness of high-temperature molten salts requires corrosion-resistant materials to protect CSP system components over extended operational cycles [36]. Temperature-dependent viscosity changes introduce complexity in the CSP

 doi:10.20944/preprints202501.0091.v1

system design, necessitating precise control mechanisms to maintain optimal thermal and flow dynamics, which is crucial for operational efficiency and component longevity [20]. Managing viscosity variations is essential to ensure efficient heat transfer and minimize component wear due to fluctuating flow rates. In CSP setups, especially those using solar salts, reduced viscosity at higher temperatures aids smoother flow but also demands robust materials and design strategies to address thermal stress and potential corrosion at elevated temperatures [37]. Moreover, understanding the risk of molten salt solidification is vital for guiding design and operational conditions in CSP plants [11]. Key components like pressure sensors and bellows seal globe valves are crucial for monitoring and controlling operational parameters. These components help maintain safe operational pressure levels and regulate fluid mass flow rates, ensuring the optimal functioning of the TES system. During system startup and commissioning, pressure sensors may experience thermally induced drift due to environmental variations and fluid heating, affecting system accuracy and performance. In the development and testing of components for molten salt TES systems within CSP facilities, effective performance across a broad temperature range is crucial [38]. Rodriguez-Garcia et *al.*[39] conducted tests on commercial globe valves and pressure transmitters at high temperatures to improve component design and adaptability for molten salt TES systems. Similarly, Peirò et *al*. [40] explored materials, components, and operational strategies for TES systems up to 400°C, identifying challenges like leaks and salt solidification, particularly at cold spots. They highlighted the importance of proper electrical heat tracing systems (EHTS) and insulation, especially in smaller-scale plants prone to significant heat losses and reduced thermal inertia. Protection of signal wires against disturbances and high temperatures is essential to maintain system functionality. While radar level meters are effective, their high sensitivity to disturbances requires careful implementation. Mechanical level meters are not recommended in environments with potential salt buildup due to the risk of operational failures. Instead, the use of plate orifice flowmeters combined with high-quality pressure sensors offers a reliable solution for mass flow measurement, as bellows-type pressure sensors are unsuitable for use with molten salts. In their study, Rodríguez-García *et al.* [41] discussed essential technical considerations for the design and start-up of a molten salt pilot plant. They recommended using pipes with diameters no smaller than 4 inches to ensure adequate contact with the EHTS, crucial for maintaining system efficiency. The placement of vent valves was emphasized for safely releasing steam during startup, thereby enhancing operational safety and reliability. The study also highlighted the importance of managing thermal losses in storage tanks, particularly around flanged elements and supports that significantly impact heat retention. Special reinforced insulation is advised for these critical areas to mitigate heat loss effectively. For TES heat exchangers, attention should be paid to the drainage solution during the design phase to preserve thermal performance. Instrumentation and valve positioners lacking electronic components are preferred near heat sources to prevent overheating and ensure consistent operation. Additionally, the EHTS and insulation are critical components of a TES plant, requiring meticulous design and installation, especially around valves and supports where temperature drops are most likely. Temperature sensors for EHTS control should be placed in areas expecting the lowest temperatures to avoid false readings influenced by additional heat sources. Regular monitoring of the insulation resistance of EHTS is recommended to detect potential failures early and schedule preventive maintenance accordingly. Ding and Bauer [42] emphasize the necessity for further development and demonstration of all key components in the molten salt cycle, including storage tanks, heat exchangers, piping, pumps, and valves, through pilot tests at elevated temperatures for next-generation CSP plants. They advocate for broadening the technological scope to include materials and processes, aiming to transition from theoretical to practical applications of molten salt technology. Despite advancements, there remains a significant gap in performance characterization, reliability analysis under various conditions, and understanding of failure mechanisms, particularly concerning temperature fluctuations. These gaps are particularly pronounced in the study of critical components like pressure sensors and bellows seal globe valves. Therefore, this article introduces findings from experimental tests on these components, conducted at the ENEA Casaccia Research Centre in Rome, underscoring their

 doi:10.20944/preprints202501.0091.v1

importance and the need for extensive testing to ensure reliability and efficiency in practical applications. The primary goal of this work was to characterize the performance and reliability of the components under various operational temperature conditions, which impact the HTF viscosity. To prevent shutdowns and ensure component usability, it was necessary to heat the components actively. Such detailed characterization and rigorous testing provide crucial information that contributes to enhancing the design of these components and reducing unplanned operational downtimes in CSP plants. By thoroughly understanding the operational boundaries and failure thresholds of these key components, it becomes feasible to implement more robust and reliable systems, thereby ensuring smoother and more efficient operations of the plants. This contribution will elaborate on the methodologies used in the experimental setup, discuss the key findings, and suggest modifications for optimizing the components based on the results observed. The article is organized as follows: Section 2 defines the Materials and Methods, which includes a description of the test facility, the test preparation phase, and how the tests were conducted. Section 3 includes the results and discussion related to the circulation tests, as well as tests on the pressure sensor and bellows seal globe valves. Finally, Section 4 presents the conclusions and outlines future research.

2. Materials and Methods

2.1. MOlten Salt Experiences (MoSE) Laboratory-Scale Test Loop Description

The ENEA Casaccia Research Centre is home to a specialized facility known as MOlten Salt Experiences (MoSE), which is specifically designed for characterizing components utilized by CSP plants. MoSE operates as a laboratory-scale test loop that emulates the behavior of a CSP plant using molten salts as a HTF. The insights derived from these studies are crucial for informing the design and operation of full-scale CSP plants. Since its inception, MoSE has facilitated numerous experimental tests using a variety of salt mixtures, including both binary and ternary compositions. The MoSE facility enables the execution of dynamic corrosion resistance tests on structural materials exposed to the action of high-temperature molten salts, featuring cyclic variations over extended durations. Through this facility, suitable metallic materials can be selected and qualified, as well as testing joint elements, welds, connections between different materials, sealing elements, instrumentation, and line components that will constitute an industrial-scale CSP plant.

Furthermore, the facility also serves as an important resource for research into advanced heat transfer techniques and for the recovery and storage of high-temperature thermal energy in the industrial sector. It facilitates the easy verification of heat exchange coefficients and the exploration of the mechanical behavior of devices subjected to the action of molten salts with prolonged and cyclic temperature variations.

Entirely designed by ENEA, featuring several innovative solutions, the facility has been operational since 2003. Initially, the infrastructure was used to assess the suitability of AISI 321H and AISI 316T stainless steels for the Archimede solar power plant [43] (developed by ENEL using ENEA technology). Tests were conducted for up to 8,000 hours of continuous operation, with daily heating and cooling cycles, which allowed for the validation of the chosen steels and their welding procedures.

Figure 1 offers two distinct views of the MoSE facility: Figure 1 (a) a comprehensive view of the entire MoSE loop, highlighting the layout and overall structure, and Figure 1 (b) a perspective from the control room, providing insight into the sophisticated monitoring and control systems implemented.

 doi:10.20944/preprints202501.0091.v1

(a) (b)

Figure 1. (a) Comprehensive view of the MoSE laboratory-scale test loop, (b) view of the plant from the control room.

Figure 2 presents the schematic layout of the MoSE laboratory-scale test loop, delineating its key components. These include a storage tank outfitted with six horizontal immersion heaters at the base and one vertical immersion heater. The system also incorporates a circulating pump for extracting molten salt from the storage tank, an electric heater that employs the Joule effect to heat the salt to the requisite temperature, and an air cooler capable of cooling the fluid when necessary. The plant is equipped with various sensors to continuously monitor critical process parameters, such as mass flow rates, pressures, and temperatures.

In the diagram, two components are marked with red circles: the Pressure Sensor (PS.1.01) and the Bellows Seal Globe Valve (VI.9.01). These elements are the focus of the experimental campaign and are the subject of this study.

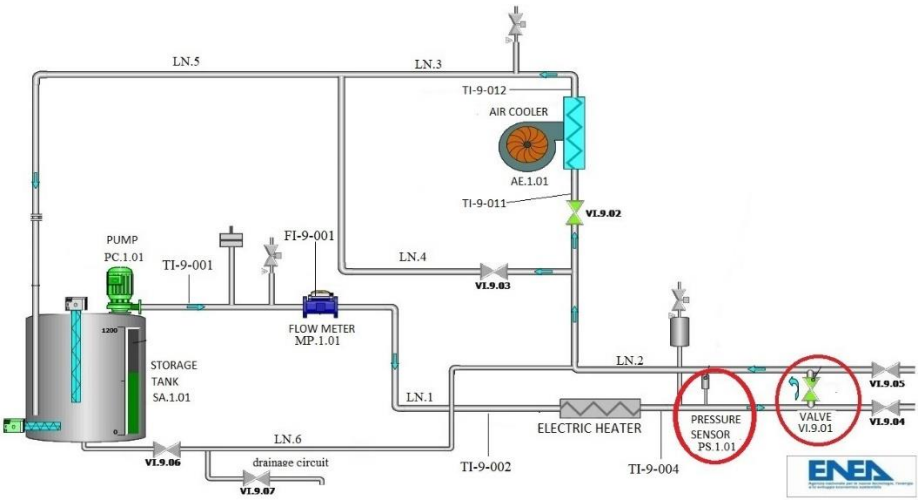

Figure 2. Overview of process showing lines and main components of the plant. In red circles the Pressure Sensor and the Bellows Seal Globe Valve considered in this analysis.

Table 1 provides a summary of the plant's main components along with their key characteristics, offering a comprehensive overview of the plant's operational features and capabilities.

Table 1. Overview of the main plant components.

Tag	Component	Notes
SA.1.01	Storage Tank	Diameter: 1000 Height: 1000
PC.1.01	Circulation Pump	Nominal power 5.5 kW
CE.1.01	Electric Heater	Joule heating effect heater, Nominal power 60 kW

 doi:10.20944/preprints202501.0091.v1

MP.1.01	Flow Meter	Ultrasonic flowmeter
AE.1.01	Air Cooler	Nominal power 5.5 kW
VI.9.01	Bellows Seal Globe Valve	DN 1“Bellows Seal Globe Valve
PS.1.01	Pressure Sensor	NaK pressure transmitter

Figure 3 presents an image of the piping, labeled as LN.1 in Figure 2, which illustrates the positions of the pressure sensor and the bellows seal globe valve, indicated by two red circles.

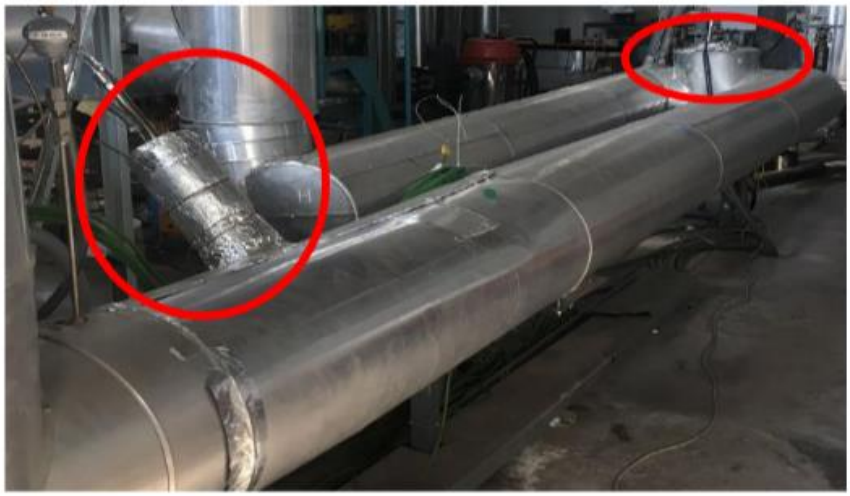

Figure 3. A detail view of the piping line containing the pressure sensor and the bellows seal globe valve considered in the study.

The necessity for the experiments described in this contribution stems from observations indicating that while globe valves equipped with ceramic packing seals on the operating shaft have demonstrated no issues with the draining of molten salt, traditional packing seals have shown significant problems. These issues often arise from the need to avoid substantial carbon presence, typically found in graphite-based materials at the temperatures involved, where it is used solely as a lubricant in minimal quantities on the ceramic packings. Such conditions can lead to molten salt leaking through the valve stem, occasionally resulting in the breakage of heating cables. Tightening the packings can prevent further molten salt leaks but at the cost of restricting the functionality of motorized stem operations. As a result of such complications, an exhaustive analysis of the components has steered the selection towards the adoption of valves with integral bellows seals. These valves ensure the complete containment of the molten salt but necessitate constant temperature regulation due to the bellows' sensitivity to the freezing of the molten salt within them. Therefore, it is critical to employ easily removable insulating and heating shells that are thoughtfully designed. The simplicity of disassembling the insulation for frequent maintenance substantially lowers costs, effectively offsetting the initial investments.

For pressure measurement, systems that use steel diaphragms with diathermic oil as an intermediary fluid have been evaluated in past experiments at ENEA Casaccia's "Prova Collettori Solari – PCS" test facility. This pilot plant is designed for experiments with molten salts as a heat transfer fluid in linear parabolic trough collector technology. Given the maximum temperature limitation of 300°C for this configuration, it was imperative to use specially sized branch nozzles to maintain the contact temperature with the sensor diaphragm below its maximum operational limit under all conditions. To prevent the accumulation of molten salt during the plant's draining process, the nozzles were vertically oriented relative to the pipes and positioned at the top, thereby enhancing drainage. During operation, this setup facilitated the creation of an air cushion between the membrane and the sensor diaphragm. Additionally, the nozzle was equipped with an EHTS independent of the system used for the originating pipe.

 doi:10.20944/preprints202501.0091.v1

However, this solution resulted in increased costs and proved to be inadequate under all operational conditions, particularly at high plant temperatures (approaching 600°C), when excessive insulation of the branches led to an increase in sensor temperatures, causing malfunctions. The system also faced calibration challenges, being highly susceptible to environmental conditions and the progressive deterioration of the insulation. In response to these challenges, the decision was made to implement a new generation of sensors, as described in this work.

2.2. Test Preparation Phase

The solar salt mixture used in this process possesses a relatively high solidification temperature, which ranges between 220°C and 240°C. To prevent the salt from cooling below this critical threshold, all components of the plant—including piping, valves, instruments, and other relevant elements—were outfitted with external EHTS, or were heated through the Joule heating effect. During the experimental tests, the operation of the EHTS was managed by the operator via the Distributed Control System (DCS). Each heating cable mounted on the components could be selectively activated or deactivated based on the specific requirements of each test being conducted.

The experimental tests were conducted within a HTF temperature range of 260°C to 550°C. The flow rate varied from approximately 0.3 to 0.5 l/s, reflecting the design specifications of the circulation pump installed on the MoSE test loop . Table 2 provides a detailed summary of the composition and the main physical properties of the solar salt mixture, specifically within the temperature range of 290°C to 550°C, utilized in the MoSE laboratory-scale test loop.

Table 2. Main properties of the used molten salt mixture [44].

Item	Value	Unit
Composition	60 wt.% $NaNO_3$ - 40 wt.% KNO_3	•
Density	1906-1746	kg/m^3
Specific heat	1.49-1.54	kJ/ (kg °C)
Viscosity	3.55-1.2	mPa s
Conductivity	0.49-0.54	W/ (m °C)
Heat of fusion	161	kJ/kg
Initial solidification temperature	221	°C
Initial crystallization temperature	238	°C

Before initiating the tests, a multi-step process was followed to prepare the molten salt mixture for insertion into the tank. Initially, the tank itself was readied by inspecting key components such as the circulation pump, the internal electric heaters, and various pieces of instrumentation, including thermocouples, pressure sensors, and level sensors. The measuring devices installed in the tank are non-certified type K thermocouples, with an accuracy of approximately 1-2°C. The process began with the solid-state salt components, which were crushed and reduced into easily manageable parts without requiring specialized equipment. These salts, in their granular solid state, were then mixed in steel containers positioned on the ground. Subsequently, these salts were incrementally transferred into the tank and subjected to melting by the tank's internal electric heaters. Throughout this stage, temperatures at different levels within the tank were meticulously monitored to ensure uniform melting. Initially, the tank was filled with a minimal amount of salts, just enough to cover the internal electric heaters. After this foundational step, the operation paused to allow for the melting of the mixture already added to the tank. Once the melting was confirmed, the addition of more mixture proceeded, carefully maintaining the correct proportions.

At this stage, the melting process of any additional solid salt was expedited by the presence of the liquid bath. Throughout the entire procedure, the internal heaters within the tank were kept active to avert any drop in the mixture's temperature, ensuring a consistent thermal environment crucial for the successful completion of the tests. Figure 4(a-b) depicts the essential stages in preparing the molten salt mixture and the tank before the tests are conducted. Figure 4 (a) illustrates the preparation

 doi:10.20944/preprints202501.0091.v1

phase of the molten salt mixture prior to tank filling, showing the salts in their granular solid state as they are ready for melting. Figure 4 (b) offers a view inside the tank, highlighting the installation of thermocouples on the external casings of the electric heaters, an essential step for precise temperature regulation.

(a) (b)

Figure 4. (a) Preparation phase of the molten salt mixture before the tank filling; (b) a view inside the tank during the installation of some thermocouples on the electric heaters external casings.

The heating of the HTF within the storage tank was monitored using thermocouples that were previously installed at various levels. Past testing experiences at the MoSE facility have shown that the temperature of the salt in the tank initially rises almost linearly over time. However, decreases in temperature have been observed when cold blocks of salt, which are gradually melting, fall into the lower bath and mix. From these observations, it was noted that the melting of the mixture typically begins at around 220°C and continues until about 240°C, at which point the molten salt mixture is completely melted. Given that the primary objective of the test campaign was to examine the behaviour of the pressure sensor and the bellows seal globe valve under varying temperatures, both components were equipped with electric heat tracing, insulated, and suitably instrumented before starting the tests, as shown in Figure 5 and Figure 6, to prevent the salt from solidifying on the components themselves.

In particular, Figure 5 (a) shows a schematic section drawing of the bellows seal globe valve, providing a detailed view of its internal components and design specifications. Figure 5 (b) displays the bellows seal globe valve during the assembly phase, where electric cables are being attached and thermocouples are welded. Finally, Figure 5 (c) depicts the bellows seal globe valve after the final assembly, showcasing the fully assembled and ready-to-use component.

 doi:10.20944/preprints202501.0091.v1

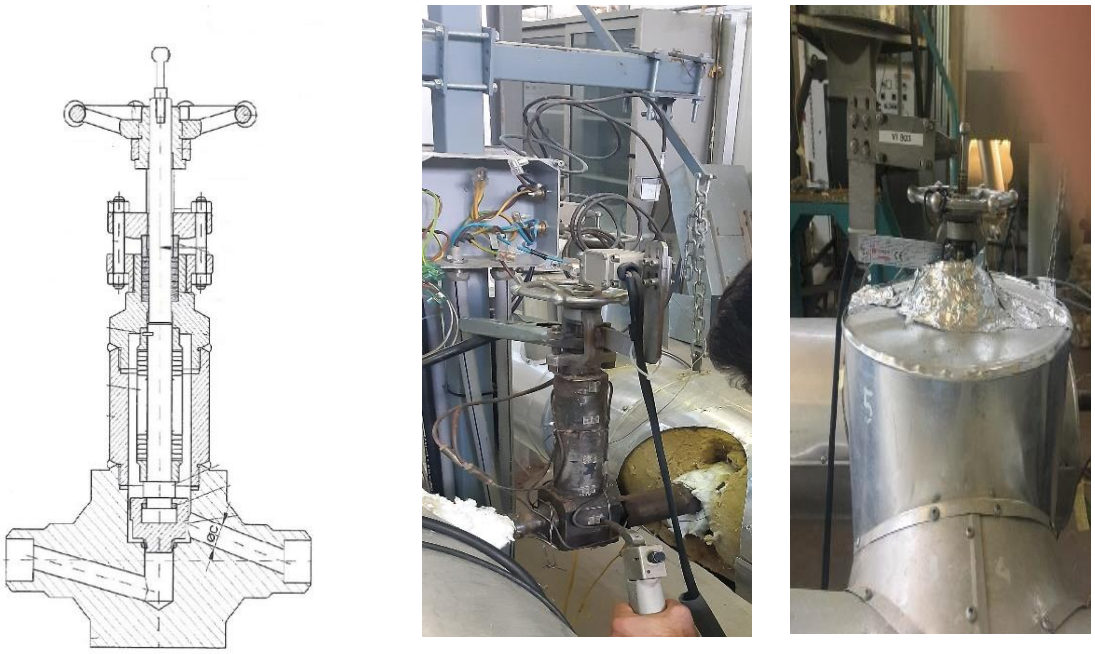

(a) (b) (c)

Figure 5. (a) A schematic section drawing of the bellows seal globe vale; (b) the valve during the electric cables assembly and the thermocouples welding on its casing; (c) the Bellows Seal Globe Valve after the final assembly.

Figure 6 provides a detailed visualization of the pressure sensor at various stages of its setup. Figure 6 (a) features a schematic drawing of the pressure sensor, offering an illustration of its structure and internal components. Figure 6 (b) shows the sensor during the assembly process, specifically when electric tracing was being assembled and thermocouples were installed. Figure 6 (c) presents the instrument after the final assembly, displaying the unit ready for use.

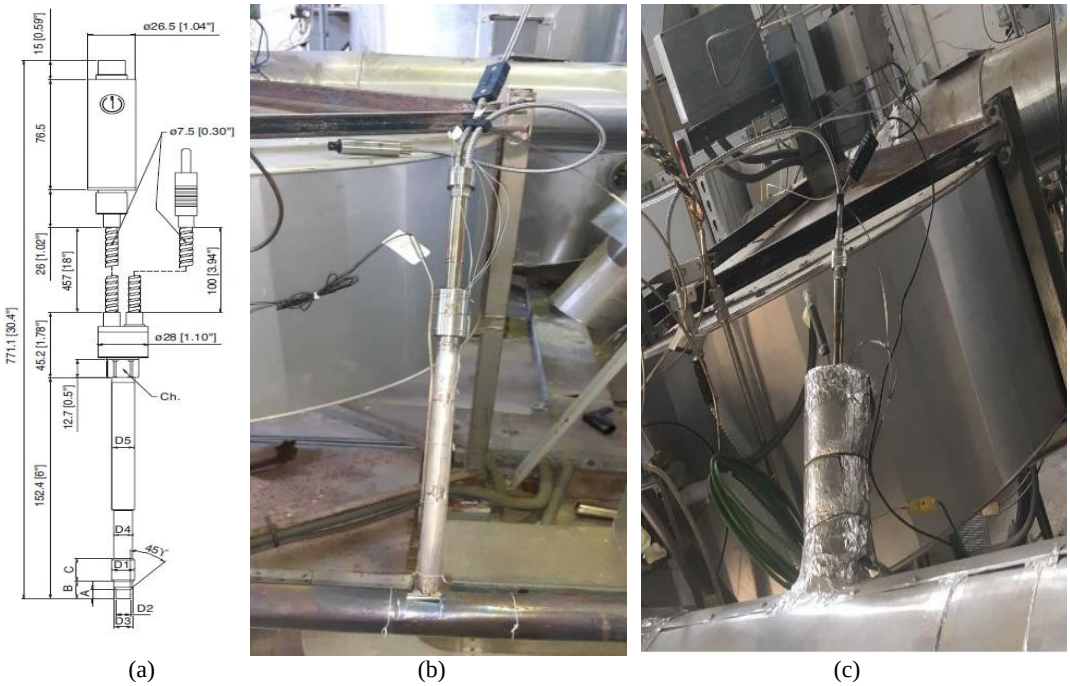

(a) (b) (c)

Figure 6. (a) schematic drawing of the pressure sensor; (b) view of the instrument during electric tracing assembly and thermocouples installation; (c) the instrument after the final assembly.

The pressure sensor functions based on the principle of hydraulic pressure transmission, utilizing an incompressible transmission liquid—specifically, a sodium-potassium (NaK) alloy. Figure 7 and Figure 8 depict the placement of thermocouples on the casings of the two components.

 doi:10.20944/preprints202501.0091.v1

To enhance temperature measurement, stainless steel sheet patches, 0.2 mm thick, were welded onto the bellows seal globe valve stem and the pressure sensor, providing a secure attachment point for the thermocouples. Subsequently, electric tracing cables were installed on both instruments to prevent the salts from solidifying. Figure 7 (a) and Figure 8 (a) provide close-up views of the bellows seal globe valve and the pressure sensor, respectively, displaying their construction and assembly details. Meanwhile, Figure 7 (b) and Figure 8 (b) present schematics of the bellows seal globe valve and pressure sensor, with indications of the thermocouples' positions on their casings and the temperatures recorded in each section.

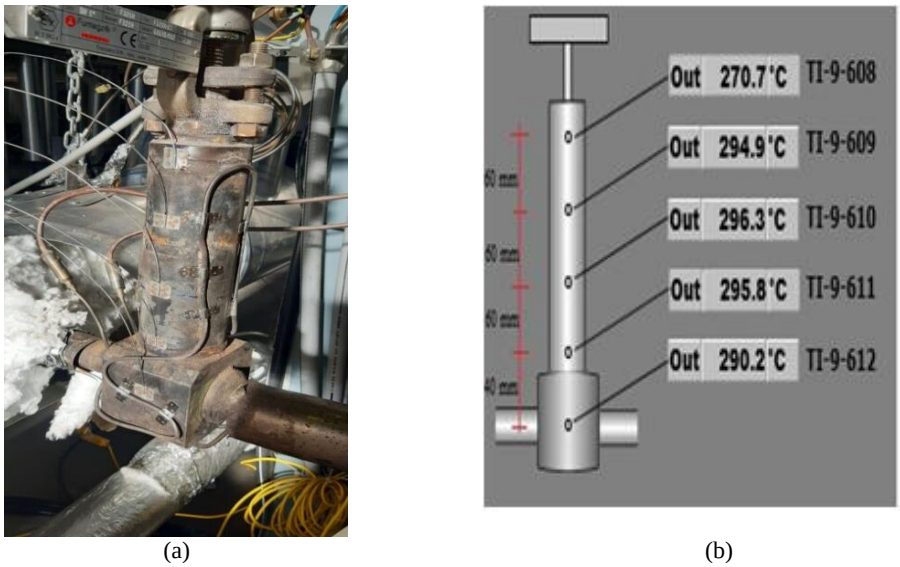

(a) (b)

Figure 7. (a) detail view of the bellows seal globe valve; (b) schematic drawing of the bellows seal globe valve with indication of the thermocouples position on its casing.

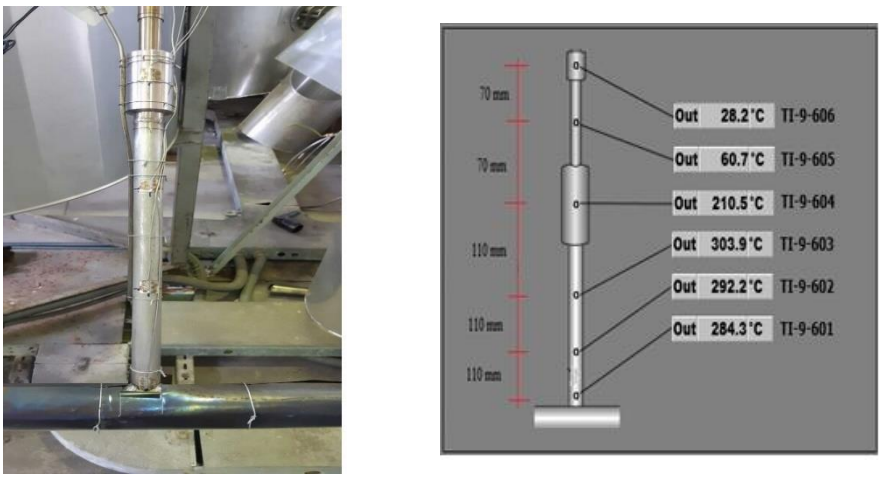

(a) (b)

Figure 8. (a) A detailed view of the pressure sensor; (b) a schematic drawing of the pressure sensor with indication of the thermocouples position on its casing.

2.3. Experimental Tests

Within the test loop, in circulation mode, the HTF flows through the salt circuit as specified by operators managing the process via DCS. Typically, the EHTS is deactivated during this phase and is controlled automatically through the DCS. However, operators can manually activate the electric heating cable on specific piping lines or components, depending on the requirements of the ongoing test. In stand-by mode, the fluid is stored in the storage tank and maintained at a minimum safety temperature by the electric heaters immersed in the fluid, while minimizing heat loss through

 doi:10.20944/preprints202501.0091.v1

insulation. In this mode, the EHTS throughout the rest of the system is automatically toggled on or off by the DCS. The experimental campaign was conducted in January and February 2023, structured into three main categories of tests, with two experiments in each. The first category, termed circulation tests, involved circulating molten salts at a fixed mass flow rate with variable initial temperatures (Test I and Test II). These tests were paired with comprehensive temperature monitoring of all pipes and system components with the EHTS consistently set to automatic mode. The starting temperatures were approximately 294 °C for Test I and 287 °C for Test II. The second category, the pressure sensor tests focused on the PS.1.01 component (Test III and Test IV), monitored temperature variations on the sensor body during normal fluid circulation, conducted at nearly the same salt flow rate, and when the electric tracing system was deactivated. Test III began with a salt temperature of approximately 510 °C, while Test IV started at a lower temperature of about 315 °C. Lastly, the third category, the bellows seal globe valves tests (Test V and Test VI), involved analysing the temperature of the bellows seal globe valve thermocouples during standby periods and after the deactivation of the electric tracing to assess the cooling rate of the salt within the component over time. The aim of these last experimental tests on the bellows seal globe valves VI.9.01 is to study its behaviour when the EHTS is deactivated and there is no salt circulation. Table 3 lists, for each test, the average mass flow rate of the salt maintained during the experiment and the initial temperature of the molten salt at the start of the test.

Table 3. Overview of process operating conditions during the circulation tests.

Test [-]	Average mass flow rate [l/s]	Starting salt temperature [°C]
	Circulation tests	
I	0.3	294
II	0.29	287
	Pressure sensor tests	
III	0.4	510
IV	0.43	315
	Bellows seal globe valves	
V	0	275
VI	0	264

3. Results and Discussions

3.1. Circulation Tests Results

Figure 9 (a) and Figure 9 (b) illustrate the outcomes of the circulation tests for Test I and Test II, respectively. These figures show temperature readings from two key locations: immediately downstream from the storage tank at TI-9-001, and just after the electric heater at TI-9-004 (refer to Figure 2 for component layout). Additionally, they display temperature trends captured by the thermocouples installed on the body of the valve at TI-9-612, which is positioned near the piping line. Temperatures at TI-9-011 and TI-9-012, located upstream and downstream of the air cooler respectively, are also depicted. The x-axis represents time in hours, minutes, and seconds. The y-axis on the left measures temperature in degrees Celsius, ranging up to 350°C, while the y-axis on the right measures flow rate in l/s. Five temperature sensors are represented by different colours: TI_9_001 (blue), TI_9_002 (red), TI_9_004 (purple), TI_9_011 (teal), and TI_9_012 (orange). Test I began at 10:55 AM with the molten salt temperature initially at approximately 290°C. The temperature profiles for most sensors show relative stability at temperatures around 300°C, with minor fluctuations over time. Two sharp dips in temperature are notable at approximately 12:24:29 and 13:22:05, where temperatures briefly plummet below 50°C before recovering. The flow rate, depicted by the green line (FI_9_001), exhibits more variability. Initially, the flow rate is stable around 0.5 l/s but experiences a significant drop to approximately 0.3 l/s at around 12:24:29, coinciding with one of the sharp temperature dips. The flow rate then varies, showing a general decline towards the

 doi:10.20944/preprints202501.0091.v1

end of the recorded period, punctuated by sporadic peaks and troughs. However, the temperatures were maintained above the molten salt's solidification point due to the continuous operation of the EHTS, which was set to automatic mode. The test concluded after about three hours.

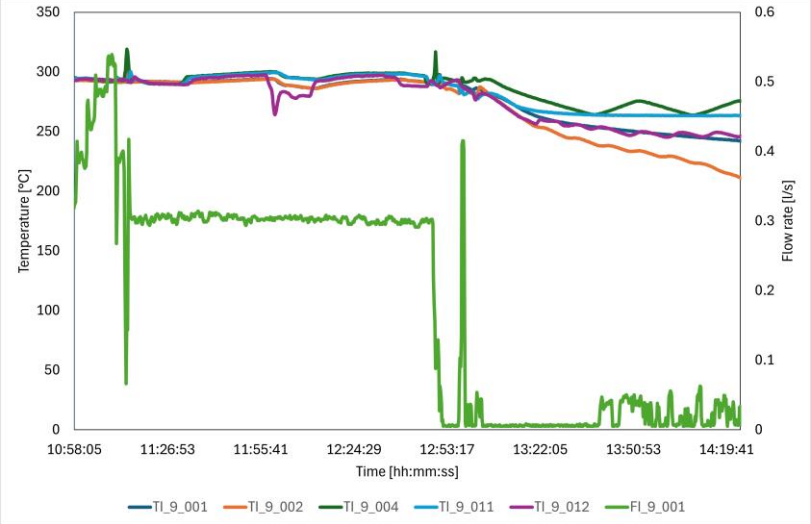

(a) Test I

(b) Test II

Figure 9. Measured temperature profiles of the salt in the piping line and on the bellows seal globe valve casing. Test I (a). Test II (b).

In Test I, the sharp reduction in mass flow rate resulted in a gradual decrease in temperatures. This potential risk to system stability was effectively mitigated by the automatic activation of the EHTS. The EHTS ensured that the temperatures remained above the critical threshold, preventing any risk of salt solidification.

In Test II, the consistent mass flow rate played a crucial role in maintaining stable temperatures throughout the duration of the test. This consistency helped keep the temperatures sufficiently high, ensuring that the molten salt remained in a liquid state and flowed smoothly without any interruptions caused by solidification.

Figure 10 (b) illustrates the temperature of the molten salt at location TI-9-004, situated in line LN.1, immediately upstream of the pressure sensor. Additionally, it presents the temperature trends recorded by thermocouples mounted on the body of the pressure sensor: TI-9-604, TI-9-603, TI-9-602, and TI-9-601, as detailed in Figure 8 (b). This visualization helps to track the temperature changes across different parts of the pressure sensor throughout the testing process.

 doi:10.20944/preprints202501.0091.v1

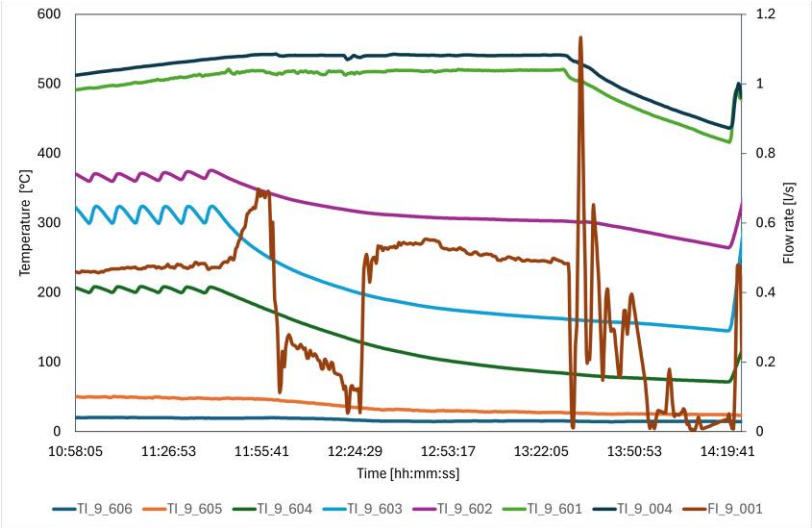

(a) Test III

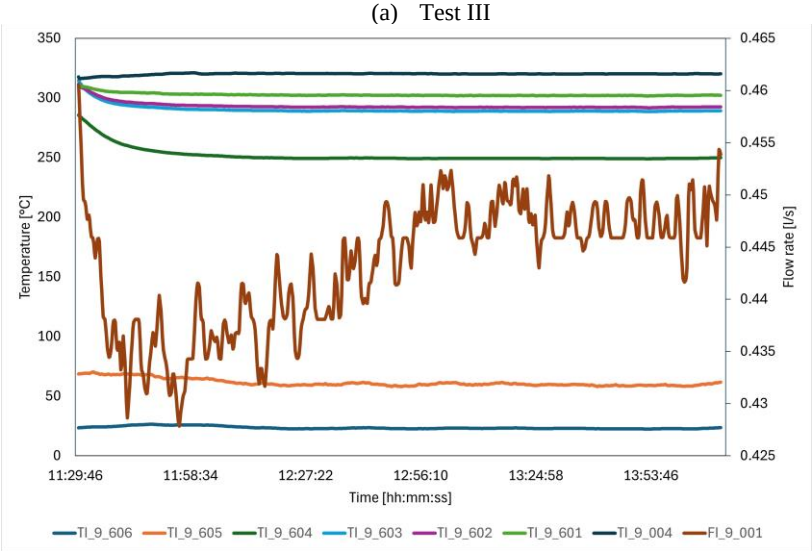

(b) Test IV

Figure 10. Measured temperature profiles of the salt in the piping line and on the pressure sensor casing. Test III (a). Test IV (b).

3.2. Pressure Sensor Tests

In Test III, the analysis incorporates both the temperature of the molten salt and the readings from all the thermocouples installed on the body of the pressure sensor.

Figure 10 (a) provides a detailed graphical representation of temperature trends during Test III. The thermocouples, designated as TI-9-604 (teal), TI-9-603 (purple), TI-9-602 (brown), and TI-9-601 (orange), measure temperatures at different locations on the branch pipe of the pressure sensor. Additional thermocouples, TI-9-605 (blue) and TI-9-606 (green), positioned outside the insulation, offer comparative temperature data unaffected by direct heat tracing influences. The flow rate is illustrated in green, depicting changes over the test duration. Initially, from 10:56 to 11:40, the EHTS's intermittent activation influenced temperatures notably on the branch pipe sensors TI-9-604, TI-9-603, and TI-9-602. These sensors demonstrated temperature fluctuations around 200°C, 300°C and 380°C respectively. TI-9-601, closer to the high-temperature fluid flow, remained relatively stable, with a slight variation around 500°C. When the EHTS was turned off post-11:40, the temperatures of TI-9-604, TI-9-603, and TI-9-602 saw a gradual decline. A critical moment occurred at 13:30 when the mass flow rate, initially steady at about 0.5 l/s, dropped sharply to nearly 0.1 l/s. This reduction coincided with a dramatic decrease in temperatures at TI-9-004 and TI-9-601, which dropped to around 100°C and 450°C respectively. The heating system was briefly reactivated at 14:19, leading to

 doi:10.20944/preprints202501.0091.v1

a temporary increase in temperatures across all sensors before it was turned off again. The temperatures at TI-9-603 and TI-9-604, further from the heat source, fluctuated more widely, while TI-9-605 and TI-9-606 outside the insulation displayed stable temperatures between 500°C and 550°C, less affected by EHTS changes. The test concluded at 14:30, emphasizing the importance of heat tracing and sensor placement in EHTS management in maintaining optimal operational conditions of the component within a CSP systems.

Figure 10 (b) depicts the temperature and flow rate data during Test IV, focusing on the operational dynamics of the pressure sensor system. Initially, the test began with the heating system set to maintain the pressure sensor's temperature above 240°C to prevent the molten salt from solidifying. The figure shows that after an initial adjustment period, the temperatures stabilized, illustrating effective control by the heating system. Throughout the test, the temperature readings for TI-9-601 and TI-9-004, positioned near the flow of molten salt, exhibited similar trends, indicating direct thermal influence from the salt's temperature. Specifically, the temperature of TI-9-004 started from a higher initial reading and experienced a gradual decrease to stabilize around 300°C. Similarly, TI-9-601, due to its proximity to the tube carrying the hot molten salt, as illustrated in Figure 8, closely followed this trend, indicating that it was significantly influenced by the heat transfer from the flowing molten salt. The flow rate, represented by the green line labelled FI_9_001, remained nearly constant throughout the test, hovering around 0.45 l/s, which suggests a steady state was maintained in the system's operational parameters. This stability in flow rate was crucial for maintaining consistent temperature readings across the monitored components. The test concluded at 14:05, with the final readings showing that the system's temperatures had effectively been maintained above the critical threshold, thanks to the precise regulation of the heating system and the stable flow rate of the molten salt. This setup ensured that the sensor and the salt temperatures remained within safe operational limits, preventing any freezing or damage due to low temperatures.

3.3. Bellows Seal Globe Valve Tests

Figure 11 (a) and Figure 11(b) present the results of the bellows seal globe valves tests. In both figures, the blue line represents the temperature data from sensor TI_9_608, while the orange and red lines depict the readings from TI_9_609 and TI_9_610, respectively. The teal and purple lines correspond to TI_9_611 and TI_9_612, illustrating their temperature profiles during the test. Additionally, the green line indicates the ambient temperature, captured by TI_9_615_Amb, which serves as a reference for the external environmental influences on the system.

As displayed in Figure 11 (a) the test initiated at 09:38. By 09:57, after deactivating the heat tracing system of the bellows seal globe valve, temperatures were recorded between 264°C and 281°C. Subsequently, temperatures began to decline, falling below 240°C, which made manipulating the bellows seal globe valve by turning the handwheel increasingly difficult. By 11:07, the handwheel had become immovable, suggesting that the salt within the bellows seal globe valve—specifically the fluid in contact with the bellows—was approaching a frozen state. At this critical point, temperature readings at various sensor locations were: 205°C at TI-9-609, 212°C at TI-9-610, and 223°C at both TI-9-611 and TI-9-612. To mitigate the risk of system failure due to low temperatures, the heat tracing system was promptly reactivated. This action resulted in a gradual and steady increase in temperatures across all monitored points. By 11:50, temperatures had risen above 250°C, restoring full functionality to the bellows seal globe valve. This sequence highlights the critical importance of temperature management in maintaining operational integrity in systems susceptible to freezing.

 doi:10.20944/preprints202501.0091.v1

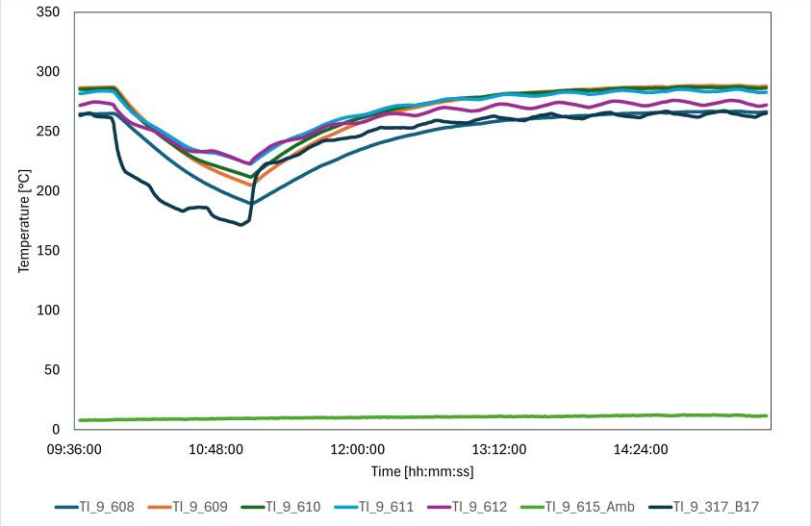

(a) Test V

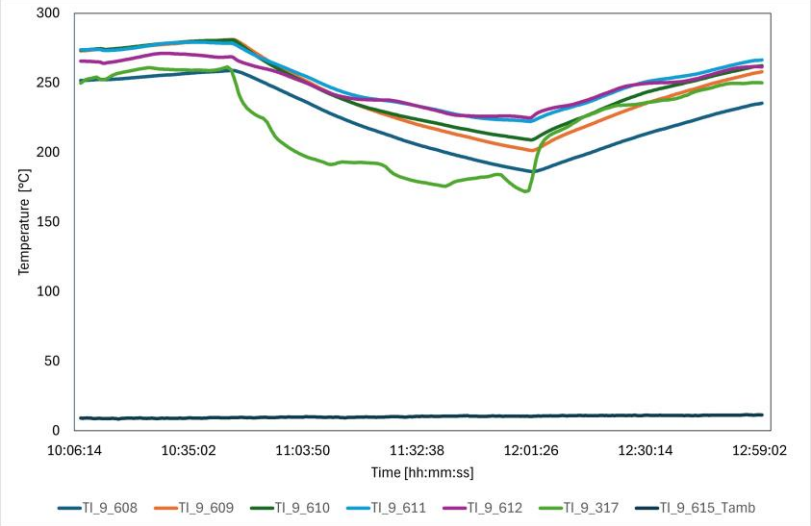

(b) Test VI

Figure 11. Temperatures trend on the bellows seal globe valve body vs time. Test V (a). Test VI (b).

Figure 11 (b) presents the temperature profiles during the second iteration of Test VI, providing a detailed analysis of thermal dynamics within the experiment. This visualization effectively captures the fluctuations and variations in temperature, crucial for evaluating the performance of the bellows seal globe valve under different operational conditions. The test commenced at 10:07 AM, and by 10:46 AM, the heat tracing system for the bellows seal globe valve was deactivated. At this time, the temperatures across the system were recorded between 261°C and 278°C. With the heat tracing system turned off, the temperatures began to decrease, progressively complicating the operation of the valve's handwheel. By 12:01 PM, turning the handwheel became impossible, with temperatures at sensors TI-9-609, TI-9-610, TI-9-611, and TI-9-612 dropping to 201°C, 209°C, and 224°C respectively for the latter two. In response, the heat tracing system was reactivated, leading to a gradual recovery in temperatures. By 12:53 PM, temperatures had increased to above 250°C, thereby restoring full functionality to the bellows seal globe valve. It is critical to note that when temperatures near the salt's solidification point, careful handling of the bellows seal globe valve is imperative. Excessive force during such conditions can cause damage to the valve bellows, potentially rendering the valve inoperable and leading to significant maintenance challenges. This test underscores the importance of precise thermal management in maintaining the operational integrity of critical components within such systems.

4. Conclusions

 doi:10.20944/preprints202501.0091.v1

This article reports on experimental tests conducted at the ENEA Casaccia Research Center's MoSE test facility, focusing on a pressure sensor and a bellows seal globe valve tailored for molten salt applications in CSP plants. The primary aim of these experiments was to comprehensively evaluate the performance and reliability of these components under various operating conditions, particularly in relation to temperature fluctuations. The study incorporated three different types of tests, each performed in two distinct runs. Key findings from these tests are summarized as follows:

- The circulation tests highlighted the efficacy of electric heat tracing systems installed on the piping, instruments, and valves. These systems were effective in maintaining temperatures above the solidification point of the molten salts, thereby preventing the salts from freezing, even at low flow rates. This feature is crucial for ensuring continuous operation in environments where precise temperature control is paramount. The results are vital for refining the design and maintenance protocols of CSP plants, aiming to boost their efficiency and reliability across various operational conditions.
- The tests on bellows seal globe valves in a stand-by state, specifically when the pump was inactive, yielded notable insights. It was observed that the molten salt within the valve tends to solidify if the heat tracing on the valve body is deactivated. By manually manipulating the handwheel of the bellows seal globe valve during these tests, researchers were able to precisely identify the temperature at which the salt begins to solidify. This experimentation enabled the establishment of a critical temperature threshold, vital for preventing the freezing of molten salt in these valves. Understanding this threshold is crucial for ensuring the operational integrity and longevity of such valves in CSP plants, where meticulous temperature control is a key component of system functionality.
- The manual operation of valves, particularly when adjusting the handwheel of a manual valve, requires caution, especially as temperatures near the solidification point of molten salts (below 240°C). At these lower temperatures, the risk of damaging the bellows increases, potentially leading to salt leakage. This issue has been observed in drain valves within commercial CSP plants, where salt leakage has resulted in the need for plant shutdowns for maintenance. These incidents highlight the necessity for meticulous temperature monitoring and precise operational procedures to prevent damage and ensure the ongoing reliability of the plant's thermal management system.
- The tests provided crucial insights into the design requirements for CSP plant components, highlighting the need for a dedicated heating system independent from the piping's heating system. This requirement stems from the observation that during normal circulation, while components are exposed to the high temperature of the process HTF, areas furthest from the piping can experience temperature drops down to critical levels. Implementing an independent heating capability ensures that all parts of the component maintain optimal temperatures, thus preventing performance degradation or failure due to freezing. This design strategy is essential for maintaining the reliability and efficiency of the thermal management system in CSP operations.

The testing process also facilitated the recording of temperature values at various points on the components, which proved instrumental for designers in strategically positioning temperature sensors. These sensors play a critical role in the tracking control system, providing the controlled values necessary for precise monitoring and adjustment of the system. This detailed temperature mapping enhances the optimization of sensor placement, ensuring comprehensive coverage and precise control over the operational parameters. Such meticulous attention to sensor positioning is vital for maintaining the integrity and efficiency of the system, ensuring that all functional aspects are monitored and regulated effectively.

Future studies are scheduled to further investigate how variations in the molten salt mass flow rate affect the behaviour of different system components. These investigations will seek to determine the optimal flow rate that ensures all parts of the circuit maintain temperatures above critical thresholds while also minimizing electricity consumption.

Author Contributions: Conceptualization, methodology, supervision, formal analysis, investigation, resources, data curation, writing—original draft preparation, writing—review and editing, visualization, project administration, funding acquisition **V.R.**; methodology, formal analysis, investigation, resources, data curation, writing—review and editing, supervision, **G.P.**; writing—original draft preparation, visualization, writing—review and editing **F.R.**; data curation, resources, software, **M.G.**; data curation, validation, software **G.N.**;

 doi:10.20944/preprints202501.0091.v1

conceptualization, methodology, supervision **G.G.**; conceptualization, methodology, formal analysis, investigation, supervision, data curation, writing—original draft preparation, writing—review and editing, visualization, project administration, funding acquisition **W.G.**. All authors have read and agreed to the published version of the manuscript.

Funding: This research was funded by CSP ERA-NET EuroPatmos Project, grant number 838311 under European Union's Horizon 2020 Research and Innovation Programme.

Data Availability Statement: Data available on reasonable request.

Conflicts of Interest: The authors declare no conflicts of interest.

References

1. WMO *State of the Global Climate in 2022. WMO-No. 1316*; 2023;
2. Eurostat EU Economy Greenhouse Gas Emissions: -5.3% in Q2 2023 Available online: https://ec.europa.eu/eurostat/web/products-eurostat-news/w/ddn-20231115-1 (accessed on 12 December 2023).
3. European Commission *REPowerEU*;
4. Rana, M.M.; Uddin, M.; Sarkar, M.R.; Meraj, S.T.; Shafiullah, G.M.; Muyeen, S.M.; Islam, M.A.; Jamal, T. Applications of Energy Storage Systems in Power Grids with and without Renewable Energy Integration — A Comprehensive Review. *J. Energy Storage* 2023, *68*, 107811.
5. Meraj, S.T.; Yu, S.S.; Rahman, M.S.; Hasan, K.; Hossain Lipu, M.S.; Trinh, H. Energy Management Schemes, Challenges and Impacts of Emerging Inverter Technology for Renewable Energy Integration towards Grid Decarbonization. *J. Clean. Prod.* **2023**, *405*, 137002, doi:10.1016/J.JCLEPRO.2023.137002.
6. Kennedy, K.M.; Ruggles, T.H.; Rinaldi, K.; Dowling, J.A.; Duan, L.; Caldeira, K.; Lewis, N.S. The Role of Concentrated Solar Power with Thermal Energy Storage in Least-Cost Highly Reliable Electricity Systems Fully Powered by Variable Renewable Energy. *Adv. Appl. Energy* **2022**, *6*, 100091, doi:10.1016/J.ADAPEN.2022.100091.
7. Zhang, N.; Yu, Y.; Wu, J.; Du, E.; Zhang, S.; Xiao, J. Optimal Configuration of Concentrating Solar Power Generation in Power System with High Share of Renewable Energy Resources. *Renew. Energy* **2024**, *220*, 119535, doi:10.1016/J.RENENE.2023.119535.
8. Pilotti, L.; Colombari, M.; Castelli, A.F.F.; Binotti, M.; Giaconia, A.; Martelli, E. Simultaneous Design and Operational Optimization of Hybrid CSP-PV Plants. *Appl. Energy* **2023**, *331*, 120369, doi:10.1016/j.apenergy.2022.120369.
9. Guccione, S.; Guedez, R. Techno-Economic Optimization of Molten Salt Based CSP Plants through Integration of Supercritical CO2 Cycles and Hybridization with PV and Electric Heaters. *Energy* **2023**, *283*, 128528, doi:10.1016/j.energy.2023.128528.
10. Gutiérrez-Alvarez, R.; Guerra, K.; Haro, P. Market Profitability of CSP-Biomass Hybrid Power Plants: Towards a Firm Supply of Renewable Energy. *Appl. Energy* **2023**, *335*, 120754, doi:10.1016/j.apenergy.2023.120754.
11. Prieto, C.; Blindu, A.; Cabeza, L.F.; Valverde, J.; García, G. Molten Salts Tanks Thermal Energy Storage: Aspects to Consider during Design. *Energies* **2024**, *17*, doi:10.3390/en17010022.
12. Caraballo, A.; Galán-Casado, S.; Caballero, Á.; Serena, S. Molten Salts for Sensible Thermal Energy Storage: A Review and an Energy Performance Analysis. *Energies* **2021**, *14*, 1–15, doi:10.3390/en14041197.
13. Roper, R.; Harkema, M.; Sabharwall, P.; Riddle, C.; Chisholm, B.; Day, B.; Marotta, P. Molten Salt for Advanced Energy Applications: A Review. *Ann. Nucl. Energy* **2022**, *169*, 108924, doi:10.1016/j.anucene.2021.108924.
14. Laing, D.; Bauer, T.; Breidenbach, N.; Hachmann, B.; Johnson, M. Development of High Temperature Phase-Change-Material Storages. *Appl. Energy* **2013**, *109*, 497–504, doi:10.1016/j.apenergy.2012.11.063.
15. Fiorucci, L.C.; Goldstein, S.L.; Fiorucci, L.C.; Goldstein, S.L. Manufacture, Distribution, and Handling of Nitrate Salts for Solar-Thermal Applications. *STIN* **1982**, *83*, 21625.
16. Bradshaw, R.W.; Siegel, N.P. Molten Nitrate Salt Development for Thermal Energy Storage in Parabolic Trough Solar Power Systems. In Proceedings of the 2008 Proceedings of the 2nd International Conference on Energy Sustainability, ES 2008; ASMEDC, January 1 2009; Vol. 2, pp. 631–637.

17. Bradshaw, R.W.; Siegel, N.P. Molten Nitrate Salt Development for Thermal Energy Storage in Parabolic Trough Solar Power Systems. *2008 Proc. 2nd Int. Conf. Energy Sustain. ES 2008* **2009**, *2*, 631–637, doi:10.1115/ES2008-54174.
18. Walczak, M.; Pineda, F.; Fernández, Á.G.; Mata-Torres, C.; Escobar, R.A. Materials Corrosion for Thermal Energy Storage Systems in Concentrated Solar Power Plants. *Renew. Sustain. Energy Rev.* **2018**, *86*, 22–44, doi:10.1016/J.RSER.2018.01.010.
19. Orozco, M.A.; Acurio, K.; Vásquez-Aza, F.; Martínez-Gómez, J.; Chico-Proano, A. Thermal Storage of Nitrate Salts as Phase Change Materials (PCMs). *Materials (Basel).* **2021**, *14*, 7223, doi:10.3390/ma14237223.
20. Majó, M.; Svobodova-Sedlackova, A.; Fernández, A.I.; Calderón, A.; Barreneche, C. Thermal Cycling Test of Solar Salt in Contact with Sustainable Solid Particles for Concentrating Solar Power (CSP) Plants. *Energies* **2024**, *17*, 2349, doi:10.3390/en17102349.
21. Bhatnagar, P.; Siddiqui, S.; Sreedhar, I.; Parameshwaran, R. Molten Salts: Potential Candidates for Thermal Energy Storage Applications. *Int. J. Energy Res.* **2022**, *46*, 17755–17785, doi:10.1002/er.8441.
22. Cabeza, L.F.; Martínez, F.R.; Borri, E.; Ushak, S.; Prieto, C. Thermal Energy Storage Using Phase Change Materials in High-Temperature Industrial Applications: Multi-Criteria Selection of the Adequate Material. *Materials (Basel).* **2024**, *17*, doi:10.3390/ma17081878.
23. Tong, Z.; Li, L.; Li, Y.; Wang, Q.; Cheng, X. The Effect of In Situ Synthesis of MgO Nanoparticles on the Thermal Properties of Ternary Nitrate. *Mater. 2021, Vol. 14, Page 5737* **2021**, *14*, 5737, doi:10.3390/MA14195737.
24. Li, N.; Wang, Y.; Liu, Q.; Peng, H. Evaluation of Thermal-Physical Properties of Novel Multicomponent Molten Nitrate Salts for Heat Transfer and Storage. *Energies 2022, Vol. 15, Page 6591* **2022**, *15*, 6591, doi:10.3390/EN15186591.
25. Henríquez, M.; Reinoso-Burrows, J.C.; Pastén, R.; Soto, C.; Duran, C.; Olivares, D.; Guerreiro, L.; Cardemil, J.M.; Galleguillos Madrid, F.M.; Fuentealba, E. Long-Term Evaluation of a Ternary Mixture of Molten Salts in Solar Thermal Storage Systems: Impact on Thermophysical Properties and Corrosion. *Mater. 2024, Vol. 17, Page 4053* **2024**, *17*, 4053, doi:10.3390/MA17164053.
26. Wang, H.; Li, J.; Zhong, Y.; Liu, X.; Wang, M. Novel Wide-Working-Temperature NaNO3-KNO3-Na2SO4 Molten Salt for Solar Thermal Energy Storage. *Mol. 2024, Vol. 29, Page 2328* **2024**, *29*, 2328, doi:10.3390/MOLECULES29102328.
27. Li, N.; Wang, H.; Yin, H.; Liu, Q.; Tang, Z. Effect of Temperature and Impurity Content to Control Corrosion of 316 Stainless Steel in Molten KCl-MgCl2 Salt. *Mater. 2023, Vol. 16, Page 2025* **2023**, *16*, 2025, doi:10.3390/MA16052025.
28. Wei, Y.; Cao, J.; Yu, H.; Sheng, J.; La, P. Effect of Mg Addition on Molten Chloride Salt Corrosion Resistance of 310S Stainless Steel with Aluminum. *Met. 2024, Vol. 14, Page 1109* **2024**, *14*, 1109, doi:10.3390/MET14101109.
29. Lei, P.; Zhou, L.; Zhang, Y.; Wang, F.; Li, Q.; Liu, J.; Xiang, X.; Wu, H.; Wang, W.; Wang, F. Corrosion Behavior of Ni-Cr Alloys with Different Cr Contents in NaCl-KCl-MgCl2. *Materials (Basel).* **2024**, *17*, 2335, doi:10.3390/ma17102335.
30. Meng, Q.; Lai, L.; Rao, W.; Li, A.; Yu, H.; La, P. Creep Properties and Corrosion Behavior of TP347H Stainless Steel with Al in Molten Carbonate Salt. *Mater. 2024, Vol. 17, Page 6108* **2024**, *17*, 6108, doi:10.3390/MA17246108.
31. Morales, M.; Gordon, S.; Fernández-Arana, Ó.; García-Marro, F.; Mateo, A.; Llanes, L.; Fargas, G. Duplex Stainless Steels for Thermal Energy Storage: Characterization of Oxide Scales Formed in Carbonate Salts at 500 °C. *Met. 2022, Vol. 12, Page 2156* **2022**, *12*, 2156, doi:10.3390/MET12122156.
32. Morales, M.; Cabezas, L.; Castro-Alloca, M.; Fargas, G.; Llanes, L.; Mateo, A. Corrosion Evaluation of Austenitic and Duplex Stainless Steels in Molten Carbonate Salts at 600 °C for Thermal Energy Storage. *Met. 2022, Vol. 12, Page 2190* **2022**, *12*, 2190, doi:10.3390/MET12122190.
33. Morales, M.; Rezayat, M.; Mateo, A. Amorphous Carbon Film as a Corrosion Mitigation Strategy for Stainless Steel in Molten Carbonate Salts for Thermal Energy Storage Applications. *Mater. 2024, Vol. 17, Page 5619* **2024**, *17*, 5619, doi:10.3390/MA17225619.

34. Arnaoutakis, G.E.; Katsaprakakis, D. Al Concentrating Solar Power Advances in Geometric Optics, Materials and System Integration. *Energies* **2021**, *14*, 6229, doi:10.3390/en14196229.
35. Bell, S.; Steinberg, T.; Will, G. Corrosion Mechanisms in Molten Salt Thermal Energy Storage for Concentrating Solar Power. *Renew. Sustain. Energy Rev.* **2019**, *114*, 109328, doi:10.1016/J.RSER.2019.109328.
36. Fernández, A.G.; Muñoz-Sánchez, B.; Nieto-Maestre, J.; Cabeza, L.F. Dynamic Corrosion Test Using LiNO3 Containing Molten Salt for CSP Applications. *Appl. Sci. 2020, Vol. 10, Page 4305* **2020**, *10*, 4305, doi:10.3390/APP10124305.
37. Khoswan, I.; Abusafa, A.; Odeh, S. The Effect of Carbon Nanotubes on the Viscosity and Surface Tension of Heat Transfer Fluids—A Review Paper. *Energies 2024, Vol. 17, Page 5584* **2024**, *17*, 5584, doi:10.3390/EN17225584.
38. Gill, D.; Kolb, W.; Briggs, R. An Evaluation of Pressure Measurement Technology and Operating Performance Using Sandia's Molten Salt Test Loop. *Energy Procedia* **2014**, *49*, 800–809, doi:10.1016/J.EGYPRO.2014.03.087.
39. Rodriguez-Garcia, M.M.; Rojas, M.E.; Pérez, M. Procedures for Testing Valves and Pressure Transducers with Molten Salt. *Appl. Therm. Eng.* **2016**, *101*, 139–146, doi:10.1016/J.APPLTHERMALENG.2016.02.138.
40. Peiró, G.; Prieto, C.; Gasia, J.; Jové, A.; Miró, L.; Cabeza, L.F. Two-Tank Molten Salts Thermal Energy Storage System for Solar Power Plants at Pilot Plant Scale: Lessons Learnt and Recommendations for Its Design, Start-up and Operation. *Renew. Energy* **2018**, *121*, 236–248, doi:10.1016/J.RENENE.2018.01.026.
41. Rodríguez-García, M.M.; Herrador-Moreno, M.; Zarza Moya, E. Lessons Learnt during the Design, Construction and Start-up Phase of a Molten Salt Testing Facility. *Appl. Therm. Eng.* **2014**, *62*, 520–528, doi:10.1016/J.APPLTHERMALENG.2013.09.040.
42. Ding, W.; Bauer, T. Progress in Research and Development of Molten Chloride Salt Technology for Next Generation Concentrated Solar Power Plants. *Engineering* **2021**, *7*, 334–347, doi:10.1016/J.ENG.2020.06.027.
43. Archimede | Concentrating Solar Power Projects | NREL Available online: https://solarpaces.nrel.gov/project/archimede (accessed on 3 December 2024).
44. Bauer, T.; Pfleger, N.; Breidenbach, N.; Eck, M.; Laing, D.; Kaesche, S. Material Aspects of Solar Salt for Sensible Heat Storage. *Appl. Energy* **2013**, *111*, 1114–1119, doi:10.1016/j.apenergy.2013.04.072.